

CNRS - Université Pierre et Marie Curie - Université Versailles-Saint-Quentin
CEA - ORSTOM - Ecole Normale Supérieure - Ecole Polytechnique

Institut Pierre Simon Laplace

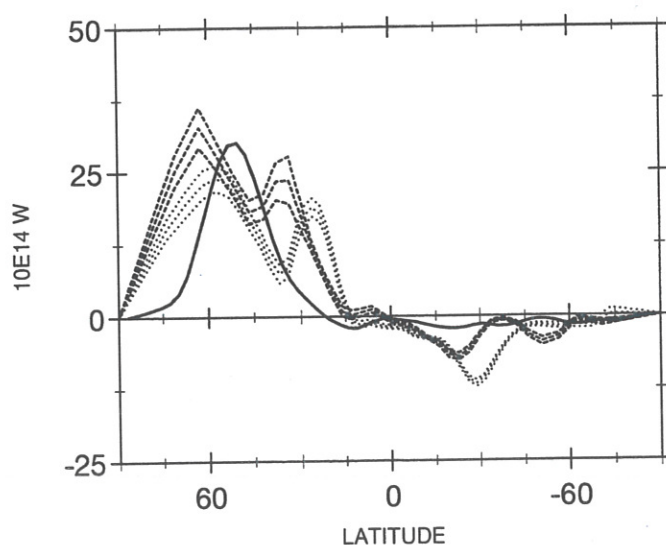
des Sciences de l'Environnement Global

Notes du Pôle de Modélisation

Impact of parameterizations on simulated winter mid-Holocene and Last Glacial Maximum climatic changes in the Northern Hemisphere

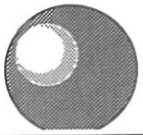
Valérie Masson, Sylvie Joussaume, Sophie Pinot
and Gilles Ramstein

Laboratoire des Sciences du Climat et de l'Environnement



Février 1998

Note n° 3

 I P S L	CNRS - Université Pierre et Marie Curie - Université Versailles-Saint-Quentin CEA - CNES - ORSTOM - Ecole Normale Supérieure - Ecole Polytechnique
	Institut Pierre Simon Laplace des Sciences de l'Environnement Global
	CETP - LMD - LODYC - LPCM - LSCE - SA

Université Pierre-et-Marie-Curie
 B 102 - T15-E5 - 4, Place Jussieu
 75252 Paris Cedex 05 (France)
 Tél : (33) 01 44 27 39 83
 Fax : (33) 01 44 27 37 76

Université Versailles-Saint-Quentin
 Collège Vauban, 47 Boulevard Vauban
 78047 Guyancourt Cedex (France)
 Tél : (33) 01 39 25 58 17
 Fax : (33) 01 39 25 58 22

Impact of parameterizations on simulated winter mid-Holocene and Last Glacial Maximum climatic changes in the Northern Hemisphere

Valérie Masson, Sylvie Joussaume, Sophie Pinot
and Gilles Ramstein

Laboratoire des Sciences du Climat et de l'Environnement

Dans le cadre du projet PMIP (Paleoclimate Modelling Intercomparison Project), nous avons effectué des simulations du climat actuel, de l'Holocène moyen (il y a 6 000 ans) et du Dernier Maximum Glaciaire (il y a 21 000 ans), à l'aide de deux versions du modèle de circulation générale atmosphérique du LMD (Laboratoire de Météorologie Dynamique, CNRS, Paris). Ces deux versions du même modèle diffèrent par leur résolution horizontale ainsi que par certaines paramétrisations des processus de surface.

Cet article présente une analyse des changements climatiques simulés aux moyennes latitudes de l'hémisphère nord, en hiver. Nous utilisons des analyses des bilans énergétiques pour diagnostiquer l'impact des paramétrisations sur la sensibilité climatique. Nous montrons que la dépendance des coefficients de transfert en surface selon la stabilité verticale de l'air joue un rôle clef pour les zones à forte stabilité : l'Atlantique nord, recouvert de banquise au Dernier Maximum Glaciaire, et les continents des moyennes latitudes pour l'Holocène. Pour cette dernière période, nous utilisons une méthode simple de projection mathématique pour extraire le signal de changement climatique de la variabilité annuelle.

Février 1998
Note n° 3

Impact of parameterizations on simulated winter mid-Holocene and Last Glacial Maximum climatic changes in the Northern Hemisphere

Valérie Masson, Sylvie Joussaume, Sophie Pinot and Gilles Ramstein

Laboratoire des Sciences du Climat et de l'Environnement

UMR CEA/CNRS 1572, Saclay, France

Tel. (33 1) 69 08 77 15

Fax. (33 1) 69 08 77 16

Email masson@lsce.saclay.cea.fr

March 2, 1998

Abstract

Within the Paleoclimate Modelling Intercomparison Project, we have performed simulations of the present-day, mid-Holocene (MH) and Last Glacial Maximum (LGM) climates with two versions of the LMD (Laboratoire de Météorologie Dynamique, CNRS, Paris) atmospheric general circulation model which differ in their horizontal resolution and some parameterizations of the surface processes. This work focuses on the winter simulated climatic changes in northern mid-latitudes and we use energy budget analyses to diagnose the impact of the parameterizations on the climatic sensitivity. The dependency of the surface transfer coefficients on the air stability is shown to play a key role for the climatic sensitivity over regions of stable conditions: the northern Atlantic which is sea-ice covered at LGM, and the mid-latitudes continents during MH. For the MH, we use a simple mathematical projection method to extract the climatic change signal from its interannual variability.

1 Introduction and numerical experiments

Differences in physical parameterizations introduced in the atmospheric general circulation models have been shown to play a key role for the simulations of present-day climate, as reviewed for instance by *Garratt* [1993], as well as on climatic sensitivity [*Mitchell*, 1990; *Gates et al.*, 1996]. Few studies have also focused on the impact of model parameterizations on past climate simulations; they have revealed the impact of soil moisture and cloud parameterizations on Holocene climate simulations [*Gallimore and Kutzbach*, 1989; *Liao et al.*, 1994; *Masson and Joussaume*, 1997]. The study by *Rind* [1988] has also illustrated the impact of the horizontal resolution on the model sensitivity, both for warm and cold climates.

One of the goals of the Paleoclimate Modelling Intercomparison Project [*Joussaume and Taylor*, 1995] is to compare the simulations of different AGCMs for two past periods (**mid-Holocene, 6 000 years ago, hereafter MH, and Last Glacial Maximum, 21 000 years ago, hereafter LGM**) in order to better understand the impacts of different parameterizations and/or resolution on model results. The MH experiment is a sensitivity study to the insolation change resulting from a different orbital configuration [*Berger*, 1978], without changes in the surface boundary conditions; in particular, there is no change in the sea surface temperatures. On the opposite, the largest forcings for the LGM experiment belong to the surface conditions: large ice caps in the northern hemisphere, changes in the ocean temperatures and sea-ice coverage, in addition to an atmospheric CO₂ reduction. In order to prepare such model-model comparisons, we have performed simulations of present-day, MH and LGM climates, with two versions of the Laboratoire de Météorologie Dynamique (LMD, CNRS-Paris) AGCMs. These two versions which have been described in *Masson and Joussaume* [1997] differ by their horizontal resolution and by their treatment of surface processes.

The first version of the LMD model used for this study is the cycle 4ter of this model. It has been used for sensitivity studies [*Le Treut et al.*, 1994] and includes a prognostic equation for cloud liquid water. The cloud scheme is indeed rather complex but the surface treatment remains crude: a simple bucket model for the hydrology, no explicit vegetation

model, surface transfer coefficients fixed for each hemisphere, each surface type (land or ocean) and each half-year (summer or winter). The snow albedo only depends on the snow depth, and the sea-ice is not fractional (either 0% or 100% of a grid cell is covered with sea-ice). This model is usually run with a low horizontal resolution (48 points in longitude and 36 regularly spaced in sine of the latitude). See *Ramstein et al.* [1997] for a description of the LGM climate as simulated by LMD4ter.

The second version used here (namely LMD5.3) is a more recent version of the LMD model, for which the surface treatments have been improved and a gravity wave drag parameterization has been implemented. The surface treatments include an explicit treatment of the vegetation with the SECHIBA land hydrology model [*Ducoudré et al.*, 1993], a parameterization of snow and ice albedo as a function of snow age, snow depth and vegetation type [*Chalita and Le Treut*, 1994]. Following the work by *Louis* [1979] for the ECMWF model [*ECMWF*, 1991], a new computation of surface transfer coefficients has been implemented for heat, snow and moisture flux, as a function of the surface type, its roughness length, the wind speed and the air vertical stability. This model version is furthermore run with a better horizontal resolution: 64 points regularly spaced in longitude and 50 points regularly spaced in sine of the latitude. So by many respects, version LMD5.3 is more complex and takes into account some physical processes in a more realistic manner. In order to better define the edges of the sea-ice, a fractional sea-ice cover has been implemented. However, this does not take into account the leads inside the sea-ice.

We have performed 16-year-long simulations of present-day, MH and LGM climates. Results have been averaged over the last 15 years of the simulations, which include the seasonal but not the diurnal cycles and allow for simple statistical evaluation of significance (Student test). As decided within PMIP, our simulations have been performed with "fixed sea-surface-temperatures (SSTs)" in order to account only for differences in atmospheric models and no ocean model. By fixed SSTs, we mean: seasonally varying monthly mean climatological SSTs, identical for each year, and based for present-day and mean Holocene on the observed present-day climatology for the period 1979-1988. Note that within PMIP.

participants have also performed an alternative simulation of the LGM climate with a mixed-layer ocean model. The changes of the LGM boundary conditions are more drastic and follow CLIMAP reconstructions [CLIMAP, 1981] for SSTs and sea-ice, and Peltier [Peltier, 1994] for ice-sheets extent (Figure 2); CO₂ has also been lowered to the glacial estimate of 200 ppm measured in the air trapped in ice cores [Raynaud *et al.*, 1993]. MH boundary conditions include a reduced CO₂ content (from 345ppm for present-day to 280 ppm as pre-industrial value) and a modified seasonal cycle in insolation (+5% insolation in summer and -5% in winter for the northern hemisphere, see Figure 1 and its caption for details).

In this work, we focus on the northern extra-tropical latitudes and we analyze the simulated climates in northern hemisphere winter (**DJF: December-January-February**) and reveal that, among other parameterizations, the dependency of the sensible heat flux transfer on vertical stability introduced in LMD5.3 is a key parameterization influencing the model sensitivity over areas where there is a change in the air vertical stability: 1) the northern Atlantic during LGM, where sea-ice replaces the open ocean, and 2) the northern mid-latitude continents for the MH. Energy budget for the dry air column is used as a diagnostic to infer such differences in the sensitivities.

2 Winter Last Glacial Maximum changes: focus over the northern Atlantic

The Last Glacial Maximum (LGM) period has been chosen for PMIP since it is an extreme cold period. Indeed, as a response to SSTs change, sea-ice extent, reduced CO₂ content, sea-level change and large continental ice-sheets, both models simulate large coolings (Figure 3) over the northern hemisphere in DJF. On the average, the northern hemisphere cools down by 3°C and the northern hemisphere lands by 4°C. We first discuss the changes over central Greenland and the Laurentide ice-sheet, and we then focus over the Northern Atlantic, where maximal temperature changes are simulated.

Over central Greenland, where estimates of paleotemperatures are available, both models simulate similar ground temperature changes of -28°C in DJF, with an annual mean

temperature changes of -20°C . However, due their different simulations of the thermal inversion, they simulate quite different surface air temperature changes: LMD4ter simulates a much larger surface air temperature decrease (-29°C in DJF, -20°C in annual mean) than LMD5.3 (-18°C in DJF, -15°C in annual mean). The classical temperature estimates from isotopic measurements in Greenland deep ice cores indicate an annual temperature change of -10°C , whereas inversion of bore-hole temperature profiles in the cores indicate about -20°C [Johnsen *et al.*, 1995]. The comparison with reconstructed LGM Greenland temperatures is nevertheless biased by the prescribed higher elevation of the ice cap [Peltier, 1994]. Indeed, Peltier reconstruction allocates $+600\text{m}$ on the average for Greenland during LGM, whereas indications from measurement of the air volume in the ice as well as Greenland ice-sheet numerical simulations suggest a few less hundred meters under glacial conditions [Raynaud *et al.*, 1997]. Over the Laurentide, LMD4ter simulates a maximum temperature change of -8.7° over a place of $+1500\text{m}$ orography change, located westward of the Laurentide summit. Over the same region, LMD5.3 simulates a higher temperature change (-19.4°), at the location of the maximum elevation change; in this case, the temperature change is larger than expected from the atmospheric lapse rate.

Nevertheless, the regions of maximal temperature change are located over the Northern Atlantic, where LGM sea-ice replaces present-day open ocean, but not over the ice-sheets. Indeed, large continental ice-sheets replace areas which are already cold and snow-covered during winter for present-day climate, which induces limited temperature changes (-5°C for LMD4ter, -10°C for LMD5.3 due to the higher albedo computed by LMD5.3 over ice-covered regions). On the opposite, present-day North Atlantic undergoes a complete change at LGM. Present-day mild winter conditions leading to the strong cyclogenesis are replaced by a southward extent in sea-ice, which induces much colder local temperatures. The air temperature change simulated by the two models is different: LMD4ter simulates a much larger cooling (-30°C) than LMD5.3 (-15°C) in surface air temperature. Our study will thus focus on northern Atlantic (between 50°N and 65°N), which is covered by only 5% of sea-ice in DJF for present-day and more than 97% for the LGM. The choice of the northern Atlantic

region for the comparison of the two models results from the maximum winter temperature change and from the maximum model-model difference occurring over this region.

2.1 Energy budget analysis methodology

In order to highlight the impact of the model parameterizations on the simulated climate, we use diagnostics of energy budget analyses performed for the dry air column; the coupling with the water cycle appears through the latent heat release due to the atmospheric condensation. The heat budget can be written:

$$Q^{heat} = Q_{clear}^{rad} + Q_{cloud}^{rad} + SH + LP, \quad (1)$$

where all the fluxes are counted positively for the air. Q^{heat} is the net dry static energy source for the air column (or the vertically-integrated heat advection divergence): Q_{clear}^{rad} is the clear-sky (without clouds) radiative budget (net top-of-atmosphere minus net surface short-wave and long-wave radiative flux), Q_{cloud}^{rad} the cloud radiative forcing (difference of the cloudy and clear-sky radiative budgets), SH the surface sensible heat flux from the surface to the air, LP the latent heat release due to the atmospheric condensation [Masson and Joussaume, 1997]. For each model version, each region and each flux, univariate 95% confidence intervals have been calculated from a Student test, and the differences between models for present-day which are statistically significant are noted in Table 1.

We have also analyzed the surface energy budget:

$$Q^{surf} = Q_{clear}^{rad,surf} + Q_{cloud}^{rad,surf} - SH - LE, \quad (2)$$

where Q^{surf} is the net heat budget at the surface; $Q_{clear}^{rad,surf}$ is the net incoming clear-sky (without clouds) radiative budget at the surface, $Q_{cloud}^{rad,surf}$ the cloud radiative forcing defined at the surface (difference of the cloudy and clear-sky surface incoming net radiative budgets), SH the sensible heat flux from the surface to the air and LE the latent heat release by evaporation from the surface to the air.

2.2 Simulated present-day climate in DJF: northern Atlantic energy budget analysis

Present-day northern Atlantic ocean is characterized by winter SSTs warmer than zonally-averaged surface air temperatures, due to the warm surface northward current. The overlying air is thus unstable (negative Richardson numbers in Table 1). The large latent heat release due to the condensation is mainly fed by the strong local evaporation ($LE/LP \approx 80\%$) and partly by moisture advection from southern latitudes (20%). The local energy source is due for 2/3 to the latent heat release through atmospheric condensation (cyclogenesis), and for 1/3 to the sensible heat flux from the ocean to the atmosphere; these sources largely compensate the radiative loss. The resulting net heat gain over the area is the diabatic thermal forcing of the planetary wave activity as discussed by *Held* [1983]. This energy is then transported by the eddy circulation towards the pole and the cold mid-latitude continents, where it is lost partly by the thermal radiation, partly by the sensible heat transfer from the cool air to the cold land surface (see next section).

Large differences between LMD4ter and LMD5.3 already appear for present-day northern Atlantic energy budgets. Indeed, LMD4ter simulates a three times larger heat gain than LMD5.3 for the atmosphere, due to 70% more sensible heat flux from the surface and 35% more latent heat release by the condensation. This higher condensation is itself fed by a more intense local evaporation (40% more compared with LMD5.3). The differences in surface fluxes can be related to the different model parameterizations, since LMD4ter has fixed large surface transfer coefficients. These fixed coefficients (1.40×10^{-3}) are six times larger than the northern Atlantic average of the ones computed by LMD5.3, though the local mean stratification for present-day climate simulation is unstable (mean $Ri = -1.06$). The observations by *Legates and Willmott* [1990a] suggest that LMD5.3 underestimates the precipitation over this region by a factor of 40%, whereas LMD4ter is closer to this climatology (see the caption of Table 1). Due to its strong evaporation, LMD4ter moreover simulates an atmosphere more saturated in water vapor and with more clouds. However, the cloud negative impact on the radiative budget of the air column remains marginal when

compared to the large difference in surface exchanges and in condensation.

2.3 Simulated LGM climate in DJF: northern Atlantic energy budget analysis

During LGM (Table 1), both models simulate a local sink of heat for the atmosphere over this region (-50W/m^2), instead of a present-day source of heat. LGM prescribed sea-ice cover induces stable surface conditions of the air, with a positive Richardson number and a thermal inversion between the ice and the air temperatures. For both models, the colder conditions decrease the saturation water pressure. The stable conditions induce a decrease in the transfer coefficients for LMD5.3. As a result, both models simulate an inhibition of the evaporation (decreased by one order of magnitude), and thus a decrease of the cyclogenesis due to convective activity over the northern Atlantic [Joussaume and Jouzel, 1993; Valdes and Hall, 1994]. As a result, the heat source of the air due to condensation is decreased by a factor of two. Moreover, the sign of the surface sensible heat flux is now reversed, the energy being transferred from the air to the cold surface. For both models, the contribution of the reduced condensation and the reversed sensible heat flux are quantitatively similar.

When comparing the two simulations of LGM climate over the north Atlantic in winter, large discrepancies between LMD4ter and LMD5.3 are observed. First, note that the small differences in clear-sky radiative cooling are due to the difference in albedo between the two models. Nevertheless, the largest differences appear in the sensible heat flux. As described in last subsection, LMD4ter simulates a larger temperature decrease than LMD5.3, both for the air temperature (10°C more) and the surface temperature (5°C more). Indeed, LMD4ter simulates a simultaneous cooling of the air and the surface, with a weak inversion (-1°C temperature difference between the surface and the air temperatures). On the opposite, LMD5.3 simulates a strong thermal inversion (-7°C between the surface and the air temperature). Despite the stable conditions, LMD4ter is still able to simulate a large sensible heat flux from the atmosphere to the surface (10W/m^2), which is one order of magnitude larger than for LMD5.3. This is explained by the fixed surface transfer coefficients for LMD4ter and the computed coefficients for LMD5.3. Indeed, LMD4ter surface transfer coefficients are fixed.

depending on the season (winter or summer half-year), the hemisphere and the surface type. On the opposite, for LMD5.3 these coefficients are computed [ECMWF, 1991] and depend of the surface type, its roughness length, the air stability (characterized by the Richardson number), and the wind speed. These computed coefficients decrease very quickly when air stability increase (Figure 4). Under the LGM sea-ice stable conditions, they are reduced by a factor of two when compared to present-day values and are one order of magnitude weaker than for LMD4ter.

Over the northern Atlantic during LGM, the surface turbulent flux parameterization thus seems to play a large role in the mechanisms responsible for different simulated climates. The simple parameterization used in LMD4ter induces a strong and simultaneous cooling of both the atmosphere and the surface, which are strongly coupled even in stable conditions. On the opposite, LMD5.3 is able to simulate a weak sensible heat flux under stable conditions, leading to a strong thermal inversion between the surface and the overlaying relatively warm air.

Last, note that LMD4ter simulates a LGM larger cooling of the sea-ice surface than LMD5.3, despite a less negative surface energy budget. This is a consequence of the complete ice cover assumed in LMD4ter: the negative surface budget leads to a strong decrease of the surface temperature computed over the ice, until it is ultimately balanced by the heat conduction flux inside the ice. For fractional sea-ice coverage, as present in LMD5.3 for the ocean/sea-ice limit, the largest negative heat fluxes come from the radiative cooling of the free ocean areas with higher temperatures (-1.8°). In this case, the large surface heat sink does not lead to any surface cooling, since the heat is assumed to be provided by an unlimited ocean interior heat source.

The LGM extreme cold climate thus enables us to test the impact of the dependency of the surface heat transfer coefficient on the model sensitivity. Preliminary comparison with some of the PMIP models [Masson, 1996] indicate that LMD4ter and LMD5.3 have quite extreme behaviors as far as the thermal inversion strength is concerned. Interestingly, the difference in air temperature changes simulated by these two models extends over Europe.

where the study of the simulated Fennoscandian ice-sheet mass-balance and the comparison of model results with pollen-based temperature reconstructions (Peyron, pers. comm.) may help to evaluate the realism of the simulations.

After this study devoted to one cold climatic extreme, we have focused on the other paleoclimatic period chosen for the PMIP project: the mid-Holocene (MH), six thousands years ago. Indeed, the prescribed MH insolation decreases by 5% in winter, which should induce colder conditions over the continents. Is the simulated climate change mechanism different between LMD4ter and LMD5.3? Does the surface sensible heat flux also play a key role for MH climate change? We will use the same energy budget analysis to compare the two models.

3 Winter Mid-Holocene changes at northern latitudes

We will first describe the simulated climatic changes for the mid-Holocene (MH) period, in terms of temperature and circulation changes. The insolation (Figure 1) decreases by 5% in boreal winter (reduced winter insolation in northern hemisphere, and reduced summer insolation in the southern hemisphere)¹. The MH forcing is weak, especially when compared to the large changes in the LGM surface boundary conditions, and can be seen as a perturbation of present-day climate. If the atmospheric circulation responded linearly to the insolation change, the insolation decrease should then induce a colder winter in the northern hemisphere; we will show that this depends on the model used.

Since MH climate change is only a weak perturbation of present-day climate, the question of the significance of the simulated changes cannot be avoided, especially for the mid-latitude winter circulation. We have developed a simple projection method to study the simulated interannual variability for present-day and MH. This method also enables us to select out the

¹The apparent drift in MH insolation change is due to the change in the length of the seasons and our choice to keep present-day calendar: following PMIP recommendations, we have kept the same calendar date (March, 21st) for spring equinoxes for both periods, and used classical months defined as for present-day. A less arbitrary alternative method is to define a new calendar, based on astronomical positions for each period, which would set the equinoxes and solstices in phase for both periods [Joussaume and Braconnot, 1997]. However, the choice of the calendar is not critical for DJF climatic change analysis.

simulated years which are responsible for the MH climate change signal, in order to obtain a better signal to noise characteristic for our energy budget analysis. Last, we will show with the study of energy budgets for the mid-latitude continents that the parameterization of the surface transfer coefficients also plays a major role on the model MH climatic change simulation.

3.1 Temperature and circulation changes

Both versions of the LMD model simulate in a reasonable way the averaged present-day climatic conditions over northern hemisphere in winter, i.e. the north-south and west-east temperature gradients (Figure 5), the location and intensity of pressure patterns (not shown). Like all the atmospheric models [Gates *et al.*, 1996], both models have some specific biases in simulating present-day characteristics: for instance, LMD4ter simulates too cold winter air temperatures in northern extra-tropics, whereas LMD5.3 simulates too warm winter temperatures at these latitudes (Figure 5, Table 2). These differences are associated with slightly different climates, which can be analyzed by their local energy balances and their atmospheric circulations as discussed below. As noted by Gates *et al.* [1996], improved horizontal resolution and improved treatment of the surface and atmospheric processes leads to a better simulation of present-day climate for LMD5.3 when compared to LMD4ter (earlier generation of the model) and may account for differences between the two models. The evaluation of the simulated climate does not only concern the mean patterns but also their variability and in our case the interannual variability. The comparison of simulated interannual variability with observations, which include the oceanic variability, remains limited. LMD5.3 simulates a reasonable interannual variability, but it is clear that LMD4 overestimates this interannual variability, with temperature standard deviations above 5°C over parts of northern America and Europe (not shown). This large variability in the high latitudes can be partly explained by the crude horizontal resolution at these latitudes and will also be discussed in the energy budget analysis subsection.

As a response to MH change in incoming solar radiation, both versions of the LMD model

simulate large-scale temperature decreases of a few degrees over northern hemisphere lands, mainly at low latitudes (30-60°N); this first-order response to insolation change is simulated by all the PMIP models [Masson, 1996]. At higher latitudes however, both model versions simulate areas of negative but also areas of positive temperature changes, the latter being much larger and more intense for LMD4ter than for LMD5.3 (Figure 6). The simulated atmospheric response is thus indirect with regards to the insolation forcing, which suggests a large-scale change in the planetary wave circulation. Although not within the scope of this paper, the comparison with European paleoclimatic reconstructions is possible. The European simulated warmer temperatures are also present in the most recent pollen-based European climatic reconstructions by Cheddadi *et al.* [1997]. The temperature change simulated by LMD4ter is in better agreement with these reconstructions than the one simulated by LMD5.3, which may result of chance more than of a correct climate simulation, as evidenced by the comparison of the various PMIP models results with the data over Europe Masson *et al.* [1998].

In order to better understand the temperature change described above, we now focus on the large scale circulation and the associated energy transport. In boreal winter, the main heat sources for the dry air are located in the tropics, mainly in the southern hemisphere. As a result, the total atmospheric circulation exports heat from the low-latitudes towards 1) the northern hemisphere and 2) towards the south pole. This meridional energy transport results from the mean circulation (Hadley cell) in the tropics. Over the northern mid-latitudes oceans, a secondary heat source is provided in winter by the cyclogenesis activity (see previous section). At these latitudes, the energy is transported with equal contributions by the transient eddies and the stationary eddies, the heat source being located over the relatively warm oceans and the sink over the continents. We focus mainly on the stationary wave contribution which is increased at mid-Holocene (see next paragraph).

The planetary waves can be described by studying the mean sea-level pressure patterns (Icelandic low pressure versus the Azores high pressure and the Siberian high pressure for Europe), but also by their contribution to the meridional vertically-integrated energy budget.

We have chosen the latter approach, in order to be consistent with the energy budget analysis method. The contribution of the stationary waves to the total energy transport (Figure 7a) results in a net northward transport in the northern mid-latitudes. When compared to the operational analysis model results of *Keith* [1995], both LMD4ter and LMD5.3 are able to simulate correctly the broad features of this transport, which give us confidence in the ability of the models to simulate the role of the planetary waves. However, both models overestimate the range of latitudes of the stationary contribution with two maxima surrounding the operational analysis model peak (located at 45°N); the LMD model underestimates the role of the stationary eddies at 45°N , and on the opposite overestimates the role of the transient eddies on the total transport at 45°N . This bias may be linked with the grid definition of the LMD model.

The reduced MH winter insolation reduces the heat source in the tropics but increases the heat sink over the colder northern continents (see Section 3.4) and thus the total northward energy transport. In the mid-latitudes, this increase is due to the significant enhancement of the planetary waves at 45°N (Figure 7b). MH increased meridional advection is due to the only contribution of the stationary eddies; both models simulate a one order of magnitude smaller decrease of the transient eddies contribution (not shown). Due to the enhanced planetary waves, more energy is thus transported from the mid-latitudes ocean to the surrounding continents (mainly the western coasts of northern America and Europe). Interestingly, LMD4ter simulates a much larger increase of this transport (+30% when compared with present-day intensity) than version LMD5.3 (weak but significant increase at 45°N). The increase in the stationary wave activity is associated with a large extent and deepening of the mean Icelandic low pressure towards northern Europe.

Stationary waves are indeed partly modulated by the orography, but also by the land-ocean temperature contrast. As there is no orographical forcing over Europe, the range of possible changes in the advection is larger and thus the temperature change is largest over Europe. With the fixed SSTs, decreased insolation leads to colder low-latitude continents, which in turn modulates the land-ocean contrast. The resulting intensification of the sta-

tionary waves increases in turn the energy export from the oceans to the continents. The warmer air arriving from the surrounding ocean partly loses its energy by the radiative loss, and partly transmits this energy through the surface sensible heat flux from the atmosphere towards the land surface. This climate change mechanism suggests that the MH European climatic change and the whole mid-latitude circulation might be sensitive to minor changes in the ocean conditions over the northern Atlantic (change in sea-ice extent in winter, change in the meridional SST gradient). Small SSTs changes are indeed suggested by the few available SSTs change estimates [Ruddiman and Mix, 1993] and might therefore influence climate changes at least over Europe [Masson *et al.*, 1998]. However, this is not the scope of this paper.

Since both the simulated present-day and MH atmospheric interannual variability of surface air temperatures is large over the northern high latitudes in winter, this interannual variability has to be studied to extract the signal of MH temperature change from the noise.

3.2 Interannual variability and projection method

The simulated mid-Holocene climate in response to the insolation change appears to be a weak perturbation of the present-day climate. Due to the strong interannual DJF variability, and the non-Gaussian structure of the interannual climate variables distributions, it is not possible to use the classical Student tests to evaluate the statistical significance of the simulated climate change (at the scale of each grid point). In order to better understand the signal-to-noise behavior, we have developed a simple visual method to compare the structures of the temperature patterns over northern mid-latitude continents (over the oceans, SSTs are unchanged), for each year of the control and of the MH simulations. The goal of this method is to project each simulated year on a plane formed by the mean control climate and the mean perturbed climate. We apply this analysis to the surface air temperature field which is a good indicator of mean circulation patterns over northern mid-latitudes in winter. We want to select the simulated mid-Holocene years which systematically present a DJF temperature structure different from the present-day one. This method has been inspired

by the test of the mean between model results and observations developed by *Frankignoul et al.* [1995].

Considering the spatial field associated with the mean of the 15 years of the control simulation (C) on one side, and the MH (H) simulation on the other side, we form two vectors: $\vec{C}(1, 2 \dots N)$ and $\vec{H}(1, 2 \dots N)$ with N the number of grid points in the considered region. The norm of these vectors, for instance $\|\vec{C}\| = \sqrt{\sum_{i=1}^N C_i^2}$ is the spatial quadratic mean of the temperatures over the N grid points.

Using these two vectors, we can build an orthonormal basis (\vec{u}, \vec{v}) . The first vector \vec{u} is simply formed by normalizing \vec{C} :

$$\vec{u} = \frac{\vec{C}}{\|\vec{C}\|}.$$

We now want to build a second vector \vec{V} orthogonal to the first one, with the form: $\vec{V} = \vec{H} - \alpha \vec{C}$, in order to represent the part of \vec{H} which cannot be well projected on \vec{C} . So $\vec{V} \cdot \vec{u} = 0$ and $\alpha = \frac{\vec{H} \cdot \vec{C}}{\|\vec{C}\|^2}$. Eventually we have to normalize \vec{v} : $\vec{v} = \frac{\vec{V}}{\|\vec{V}\|}$.

For one given year of one simulation, the vector formed by the field of winter temperatures \vec{X} can then be characterized by two numbers x_u and x_v which are its projection on each of the vector of the (\vec{u}, \vec{v}) basis:

$$x_u = \vec{X} \cdot \vec{u},$$

$$x_v = \vec{X} \cdot \vec{v}.$$

We have only considered a projection on two vectors (2 dimension basis). In order to rate the efficiency of this 2-D projection, we define a “score” calculated from the norm of the residuous vector \vec{R} (part of X which is not projected on the basis):

$$\vec{R} = \vec{X} - x_u \vec{u} - x_v \vec{v},$$

$$S = 100 \times \left(1 - \frac{\|\vec{R}\|}{\|\vec{X}\|}\right).$$

A 100% score would indicate that \vec{X} perfectly projects on the 2-D basis (\vec{u}, \vec{v}) .

We have used this method for LMD4ter (Figure 8) and LMD5.3 (Figure 9). The score of all these projections is for both models higher than 80%, the residuous being smaller

than both projections, indicating that our basis for the projection is thus correct. For these figures, we have centered the coordinates points so that the mean of the control simulation (C) be at the origin of the graph. Note that we have used different horizontal and vertical scales for each model so that figures be more easily readable. For LMD4ter, the different years of the control simulation form a cloud of points; 8 years out of the 15 years of the MH simulation stand outside of the set of control points; but 7 years remain among the control set of points. This means that the MH temperature change signal is due to the structure of these 8 extreme specific years. For LMD5.3, 10 out of the 15 years of the MH simulation stand outside of the control set of points. The dispersion between the different points of the control simulation is larger for LMD4ter than for LMD5.3; we have already mentioned that LMD4ter simulates a larger interannual variability. Even with only 15 years of simulated control and mid-Holocene climate, we are able to separate two distinct modes for each model.

We have compared the results of our selecting method with a similar analysis performed using not a subjective projection basis but an objective basis made by first eigen vectors of a principal component analysis; our conclusions remain unchanged. Indeed, the first empirical orthogonal function (EOF) computed from the 30 individual DJF temperature fields from both control and Holocene simulations, is close to the mean of the control years. By construction, the second EOF is orthogonal to the first one and will take into account the second mode of the interannual change in the pattern of the DJF temperature, which happens to be very close to our second vector. Unlike this EOF method, our simple method enables a 100% projection of the mean of control and Holocene years.

Taking into account the mean of the MH years which are different from control years can then help to analyze the MH climate changes by selecting the simulated years responsible for the temperature change signal, especially when specific energy budget diagnoses are required. In particular, these simulated extreme MH years ("selected years") are responsible for the presence of warmer temperatures in the mean climatic change (See Figure 6). These specific years identified by our projection method present a common structure in sea-level pressure, wind circulation, and temperature change, associated with a specific "mode" of the planetary

waves. The mean mid-Holocene change is thus associated with a deepening of the ocean-land pressure contrasts, more heat advection from the oceans to the mid-latitudes continents, warmer temperatures over northern America and Europe and colder temperatures over the tropical lands. This type of circulation happens during some simulated present-day years, but is more intense and frequent inside the distribution of the mid-Holocene years.

The mid-Holocene climatic change is thus characterized by a large-scale mid-latitudes circulation change, transporting more heat from the oceans to the continents. The insolation change being mainly seen by the atmosphere over the continents (since the SSTs are fixed), we need to analyze the heat budget over the continents to link the insolation forcing and the resulting large-scale advection change. In order to understand the mechanisms responsible for the different climatic sensitivities of LMD4ter and LMD5.3, we have analyzed the energy budgets for both the atmosphere and the surface, over the continents between 45°N and 75°N for present-day climate and for MH minus present-day change, considering only the “selected” MH years.

3.3 Present-day energy budgets

For the present-day climate (Table 2), both models show similar distributions of the energy budget of the atmosphere. The atmosphere loses energy over mid-latitude lands, due to 1) the strong thermal radiative cooling ($\approx 100\text{W}/\text{m}^2$), and 2) the sensible heat flux from the air to the surface ($\approx 30\text{W}/\text{m}^2$). The only local energy source for the dry air is the latent heat release due to condensation ($\approx 30\text{W}/\text{m}^2$), fed by the advection from the oceans (local evaporation represents less than 10% of the local precipitation). As for the surface, its energy balance over the season is null. The heat loss due to the large radiative cooling is partly compensated by the cloud greenhouse effect ($\approx 20\text{W}/\text{m}^2$) and the sensible heat flux ($\approx 30\text{W}/\text{m}^2$). The sensible heat transfer enables the warm air advected from the surrounding oceans to limit the cooling of the land surface in winter and thus plays a key role on the surface heat budget.

Despite their qualitative agreement, the two models show significant discrepancies in

the relative role of these different heat exchanges. Due to a colder tropospheric air column, LMD4ter simulates less radiative cooling of the air column than LMD5.3. Moreover, LMD4ter simulates 40% more sensible heat transfer towards the surface. This difference in sensible heat flux is associated with different air vertical profiles close to the surface: while surface temperatures are similar, LMD4ter simulates a weak vertical temperature inversion (less than 1°C between the surface and the overlying air), whereas LMD5.3 simulates a strong thermal inversion (7.7°C), associated with a large surface air stability (very high Richardson number). This difference in behavior is again directly linked with the parameterization of the surface heat transfer, as seen over northern Atlantic in LGM section. Indeed, under these stable conditions the transfer coefficients are one order of magnitude larger for LMD4ter than for LMD5.3: 7.00×10^{-3} versus 0.61×10^{-3} .

Different mechanisms thus lie behind the different present-day simulated energy budgets: LMD4ter has fixed coefficients, independently of the air stability, and is able to simulate a large sensible heat flux which cools down the air, leading to a moderate long-wave radiative cooling. On the opposite, for LMD5.3 the surface and the air are less strongly coupled, the thermal inversion is deeper and a warmer air column can persist above the cold land surface; this air loses mainly its energy by the radiative cooling. These different behaviors may account for the larger interannual variability simulated by LMD4ter compared with LMD5.3. Indeed, any perturbation of the circulation leading to more wet and cool air arriving from the ocean to the land will be able to transfer its sensible heat to the surface and induce large fluctuations in surface air temperature. On the opposite, for LMD5.3 the surface is on the average more isolated from the air; an input of warm air from the ocean will just lead to a small heat transfer to the surface and a large radiative heat loss.

3.4 Mid-Holocene change in energy budgets

During the “selected” MH period (Table 2), our region receives 4 W/m² less insolation at the top of the atmosphere (minus 5.8% when compared to present-day incoming solar radiation). The resulting temperature changes are different for the two models: LMD4ter simulates

significantly warmer surface and air temperatures, whereas LMD5.3 simulates significantly colder surface and air temperatures. The study of the change in the various terms of the energy budget is aimed at understanding the mechanisms responsible for these different climatic changes.

The change in local heat source is equal to the addition of 1) the change in local heat storage, and 2) the change in heat advection (i.e. the divergence of the heat transport). For both models, present-day heat storage over DJF is about -6.0 W/m^2 ; LMD4ter simulates a change in heat storage of $+2.2 \text{ W/m}^2$, whereas LMD5.3 simulates a smaller increase ($+0.4 \text{ W/m}^2$). Due to the increase in tropospheric air temperatures, the DJF heat storage change is positive, and the increased heat advection is larger than the local heat loss increase. Thus, the increased advection studied in previous section warms the air column and also compensates for the local heat sink. Indeed, both models simulate significant increases in the local energy loss: -8 W/m^2 (the relative change is $+8\%$) for LMD4ter, much larger than for LMD5.3 (-2 W/m^2 ; the relative change is $+2\%$). The two different climatic changes are associated with different mechanisms. We will first describe the new climate simulated by LMD4ter and then the one simulated by LMD5.3.

LMD4ter simulates a larger local heat loss due to 1) more heat transfer from the atmosphere to the land surface ($+8\%$) and 2) more radiative loss ($+6\%$). This strong heat loss is associated with an increased advection mainly resulting from the change in the heat transport by the stationary waves (see previous section). Associated with the larger heat advection, the sensible heat flux between the air coming from the oceans and the surface is able to maintain a heat accumulation in the whole air column. Indeed, the mean air temperature of the area increases by 2° ; a simple grey-body off-line calculation leads to an increased long-wave emission by about 6 W/m^2 , which is in close agreement with the simulation (5 W/m^2). As for the surface, which becomes warmer, its radiative cooling increases but is compensated for one third by the cloud radiative effects ($+6\%$) and for two thirds by the heat transfer from the atmosphere.

For LMD4ter, winter insolation changes thus induce an increased heat transport in the

northern mid-latitudes (mainly from the surrounding oceans). This advection is maintained by an increased sensible heat flux towards the surface and compensates for the increased radiative loss due to the heat accumulation in both the surface and the troposphere. Changes in the vertical stability at the surface are weak and non significant, as well as changes in the precipitation.

As for LMD5.3 now, the simulated changes are weaker and many of them do not pass the Student test performed on the average over the northern mid-latitude lands. The surface temperature changes is reversed, with a significant decrease by 1°C , an increased surface-air gradient, a higher vertical stability and a significant decrease in the surface transfer coefficient (-13%). The simulated surface cooling results almost directly from the lower local insolation, without any strong advection feedback as for LMD4ter, since the transfer of heat from the atmosphere to the surface is blocked in case of high air stability. Indeed, the sensible heat flux slightly increases but one order of magnitude less than for LMD4ter. The slightly increased advection results of the colder conditions associated with less absorbed insolation, less precipitation and a little more sensible heat flux to the surface.

To conclude, for LMD4ter the sensible heat transfer at the surface can increase even in case of vertical stable conditions, and enables the model to warm a large part of the continents in the northern latitudes: the sensible heat flux and the radiative loss, due to the warmer temperatures, maintain a strong enthalpy advection from the surrounding oceans by the stationary eddies. On the opposite, for LMD5.3, the sensible heat flux is less able to increase under stable conditions because of the surface transfer coefficient calculation. As a consequence, the climatic change reflect the local insolation change; the advection increases only slightly for this model.

Using energy budgets, we have thus suggested a mechanism which can explain the different behaviors in term of simulated temperature and large-scale circulation changes for LMD4ter and LMD5.3, over regions where the vertical stability is strong. This MH study leads to a confirmation of the results for the LGM over the northern Atlantic, for which the boundary conditions (sea-ice, ice sheets) also induce areas of strongly increased vertical air

stability.

4 Discussion and Conclusions

We thus observe similar mechanisms for simulated climatic changes occurring over thermally stable areas, both for mid-Holocene (MH) over northern continents, and for Last Glacial Maximum (LGM) over northern Atlantic. Over a surface which loses energy, LMD5.3 simulates a strong thermal inversion, and a weak sensible heat flux in stable situation. On the opposite, LMD4ter simulates a weak thermal inversion, and a strong sensible heat flux from the air to the surface, even in stable conditions.

Our comparison is certainly limited by the different horizontal resolution of the two models. Indeed, *Boyle* [1993] has shown that planetary waves cannot be correctly simulated with a low spectral resolution (T21). Future work should involve sensitivity studies to only horizontal resolution; this was not the scope of this paper, since we wanted to prepare intercomparisons within various models, which differ in many respects.

Nevertheless, the study by *Rind* [1988] emphasizes that the change in horizontal resolution mainly affects the simulated climates over the regions that are remote from direct forcings (for instance sea-ice, ice-sheets during LGM), and affects primarily the processes which are already strongly dependent on the resolution for present-day climate (precipitation...). It seems then that for our study, the horizontal resolution is not the first factor which can account for the differences between the simulated climatic mechanisms for LMD4ter and LMD5.3. A sensitivity study to the change in surface coefficients (fixed versus computed drag coefficients) has been conducted for present-day climate with a different version of the LMD5 model [*Forichon*, 1994]; the author shows that changing these coefficients induces a large impact over ice or snow-covered regions. All these elements indicate that the different treatments of surface transfer coefficients play a major role in the differences between LMD4ter and LMD5.3 over the two regions and for the two climates which we have studied.

We have shown that large uncertainties in climatic sensitivity result of different parameterizations of surface fluxes under stable conditions. In our case, the fixed oceanic conditions

have constrained the impact of such parameterizations, which play a key role on the energetics of the high latitudes. Such parameterizations have a larger potential impact on the climatic sensitivity resulting from a fully coupled ocean/sea-ice/atmospheric model. Our paleoclimatic studies under extreme cold conditions thus stress the need for a better knowledge of the surface fluxes under stable conditions, which can only be improved through observational studies devoted to present-day polar regions.

The paleoclimate simulations offer the ability to test under “extremely cold” conditions the sensitivities associated with different parameterization of the surface fluxes under stable conditions which are developed and tuned for present-day climate. It is clear that we have used two model versions with extremely different parameterizations, since one model has no stability-dependency of the surface transfer coefficients, and the other one has no lower limit in the decrease of the surface transfer coefficients under very stable conditions *Krinner et al.* [1997]. Reducing the error bar in the paleoclimatic estimations from proxy data (e.g. temperature estimates from water isotopes in Greenland ice cores, or from pollen assemblages in Europe) is necessary to estimate the realism of the climatic sensitivity.

Future work should focus on the boundary layer parameterization and its role on the atmospheric model climatic sensitivity. This sensitivity will clearly depend on the interaction of the boundary layer parameterization with the surface boundary conditions prescribed from proxy-based reconstructions. New LGM sea-ice reconstructions [*Sarnthein et al.*, 1995] indicate more open ocean in the northern high latitudes as compared with the CLIMAP indications, which could change the impact of the boundary layer parameterization on the simulated climatic change, especially for models taking into account the role of leads in the sea-ice. The analyses in term of energy budget and the projection method defined here will be of help to compare the different paleoclimatic simulations performed by the various models participating to the the PMIP project.

Acknowledgments This work has received support from EC under contract EV5V-CT94-0457. We thank the Laboratoire de Météorologie Dynamique for providing us with two versions of their atmospheric general circulation model. Simulations have been performed

at the LMCE using computing facilities provided by CEA. We thank Pascale Braconnot for fruitful discussions about statistics, projection methods and surface transfer coefficients.

References

- Berger, A., Long-term variation of daily insolation and Quaternary climatic changes. *J. Atmos. Sci.*, 35, 2362–2367, 1978.
- Boyle, J. S., Sensitivity of dynamical quantities to horizontal resolution for a climate simulation using the ECMWF (cycle 33) model, *J. Clim.*, 6, 796–815, 1993.
- Chalita, S. and Le Treut, H., The albedo of temperate and boreal forests and the northern hemisphere climate : a sensitivity experiment using the LMD GCM, *Clim. Dyn.*, 10, 213–240, 1994.
- Cheddadi, R., Yu, G., Guiot, J., Harrison, S. P., and Prentice, I. C., The climate of Europe 6000 years ago, *Clim. Dyn.*, 13, 1–10, 1997.
- CLIMAP, Seasonal reconstruction of the Earth's surface at the Last Glacial Maximum. Technical report, Geol. Soc. of Am., 1981.
- Ducoudré, N., Laval, K., and Perrier, A., SECHIBA, a new set of parameterizations of the hydrologic exchanges at the land/atmosphere interface within the LMD atmospheric general circulation model, *J. Clim.*, 6, 248–273, 1993.
- ECMWF, *Research Manual 3: ECMWF Forecast Model. Physical Parameterization*. ECMWF, Reading, UK, 1991.
- Forichon, M., Tests sur le cycle 5bis du modèle de circulation générale du LMD. Note interne 190, Laboratoire de Météorologie Dynamique, CNRS, Paris, 1994.
- Frankignoul, C., Fevrier, S., Sennechael, N., Verbeck, J., and Braconnot, P., An intercomparison between four tropical ocean models, thermocline variability, *Tellus*, 47A, 351–364, 1995.

- Gallimore, R. G. and Kutzbach, J. E., Effects of soil moisture on the sensitivity of a climate model to Earth orbital forcing at 9,000 yr BP, *Clim. Ch.*, 14, 175–205, 1989.
- Garratt, J. R., Sensitivity of climate simulations to land-surface and atmospheric boundary-layer treatments : a review, *J. Clim.*, 6, 419–449, 1993.
- Gates, W. L., et al., Climate models-evaluation, in *Climate change 1995. The science of Climate Change*, pp. 233–284, Cambridge University Press, 1996.
- Held, I., Stationary and quasi-stationary eddies in the extratropical atmosphere : theory. in *Large-scale dynamical processes in the atmosphere*, edited by B. Hoskins and R. Pearce. pp. 127–168, Academic Press, 1983.
- Johnsen, S. J., Dahl-Jensen, D., Dansgaard, W., and Gundestrup, N., Greenland palaeotemperatures derived from GRIP borehole temperature and ice core isotopic profiles. *Tellus*. 47B, 624–629, 1995.
- Joussaume, S. and Braconnot, P., Sensitivity of paleoclimate simulation results to the definition of the season, *J. Geophys. Res.*, 102, 1943–1956, 1997.
- Joussaume, S. and Jouzel, J., Paleoclimatic tracers: An investigation using an atmospheric general circulation model under ice age conditions, 2, water isotopes., *J. Geophys. Res.*, 98, 2807–2830, 1993.
- Joussaume, S. and Taylor, K. E., Status of the Paleoclimate Modeling Intercomparison Project (PMIP), in *Proceedings of the first international AMIP Scientific conference*. edited by W. L. Gates, pp. 425–430, Monterey, CA, WCRP, 1995.
- Keith, D., Meridional energy transport : uncertainty in zonal means, *Tellus A*. 47. 30–44. 1995.
- Krinner, G., Genthon, C., Li, Z.-X., and Le Van, P., Studies of the Antarctic climate with a stretched-grid general circulation model, *J. Geophys. Res.*, 102, 13731–1375. 1997.

- Le Treut, H., Li, Z. X., and Forichon, M., Sensitivity of the LMD GCM to greenhouse forcing associated with two different cloud parameterizations, *J. Clim.*, 7, 1827–1871, 1994.
- Legates, D. R. and Willmott, C. J., Mean seasonal and spatial variability in gauge-corrected global precipitation, *Int. J. of Climatology*, 10, 111–127, 1990a.
- Legates, D. R. and Willmott, C. J., Mean seasonal and spatial variability in global surface air temperature, *Theoretical and Applied Climatology*, 41, 11–21, 1990b.
- Liao, X., Street-Perrott, A., and Mitchell, J. F. B., GCM experiments with different cloud parameterization : comparisons with paleoclimate reconstructions for 6000 years BP. *Palaeoclimates*, 1, 99–123, 1994.
- Louis, J. F., A parametric model of vertical eddy fluxes in the atmosphere. *Bound.-Layer Meteor.*, 17, 187–202, 1979.
- Masson, V., Simulation du climat de l'Holocène moyen à l'aide de modèles de circulation générale atmosphérique : impact des paramétrisations, Ph.D. thesis, Ecole Centrale Paris. Chatenay-Malabry, France, 1996.
- Masson, V., Cheddadi, R., Braconnot, P., Texier, D., Joussaume, S., and participants. P.. Mid-Holocene climate over Europe: what can we infer from pmip model-data comparisons. *Clim. Dyn.*, 1998, Submitted.
- Masson, V. and Joussaume, S., Energetics of 6000BP atmospheric circulation in boreal summer, from large scale to monsoon areas, *J. Clim.*, 1997, In press.
- Mitchell, J. F. B., Greenhouse warming : is the mid-Holocene a good analogue?. *J. Clim.*, 3, 1177–1192, 1990.
- Peltier, R. W., Ice age paleotopography, *Science*, 265, 195–201, 1994.
- Ramstein, G., Serafini-Le Treut, Y., Le Treut, H., Forichon, M., and Joussaume, S.. Cloud processes associated with past and future climate change, *Clim. Dyn.*, 1997. Submitted.

- Raynaud, D., Chappelaz, J., Ritz, C., and Martinerie, P., Air content along the grip core and past surface elevation in central greeland, *J. Geophys. Res.*, 1997, accepted for publication.
- Raynaud, D., Jouzel, J., Barnola, J. M., Chappelaz, J., Delmas, R. J., and Lorius, C.. The ice record of greenhouse gases, *Science*, 259, 926–934, 1993.
- Rind, D., Dependence of warm and cold climate depiction on climate model resolution. *J. Clim.*, 1, 965–997, 1988.
- Ruddiman, W. F. and Mix, A. C., The north and equatorial Atlantic at 9000 and 6000 yr BP, in *Global climates since the Last Glacial Maximum*, edited by J. H. E. Wright, J. E. Kutzbach, T. W. III, W. F. Ruddiman, F. A. Street-Perrott, and P. J. Bartlein. pp. 94–124, University of Minnesota Press, Minneapolis, 1993.
- Sarnthein, M. et al., Variations in atlantic surface ocean paleoceanography. 50°-80°n: a time-slice record of the last 30,000 years, *Paleoceanography*, 10, 1063–1094. 1995.
- Valdes, P. J. and Hall, N. M. J., Mid-latitude depressions during the ice age. in *Long Term Climatic Variations-Data and Modelling*, edited by J.C. Duplessy and M.T. Spyridakis. volume I22, pp. 511–531, Springer-Verlag NATO ASI Series, 1994.

List of Tables

Table 1. Energy budget over the northern Atlantic ocean (60°W, 5°E, 50°N, 65°N) for present-day and LGM (no selecting). Flux are counted positively for respectively atmosphere and surface. Cloud radiative effect is computed as the difference from cloudy to clear sky radiative budgets. *, sign of the variable is not statistically significant; •, difference between LMD4ter and LMD5.3 not significant (from a 95%-level Student test). The climatology from *Legates and Willmott* [1990b] and *Legates and Willmott* [1990a] indicates a mean winter air temperature of +3°C and a mean condensational heating of 140 W/m².

Table 2. Energy budget over the northern hemisphere middle-latitude continent (180°E, 180°W, 45°N-75°N) for simulated present-day and MH climates (selected years only). Flux are counted positively for respectively atmosphere and surface. Cloud radiative effect is computed as the difference from cloudy to clear sky radiative budgets. *, sign of the variable is not statistically significant; •, difference between LMD4ter and LMD5.3 not significant (from a 95%-level Student test). The climatology from *Legates and Willmott* [1990b] and *Legates and Willmott* [1990a] indicates a mean winter air temperature of -17.8°C and a mean condensational heating of 35 W/m².

List of Figures

Figure 1. Present-day (top panel) and MH minus present-day (bottom panel) incoming top-of-the-atmosphere solar radiation (W/m^2), as a function of day (horizontal axis, starting January, 1st and latitude (vertical axis).

Figure 2. LGM change in surface elevation (m) interpolated at the resolution of LMD4ter (top) and LMD5.3 (bottom). Isolines are represented for elevation anomalies of 200, 500, 1000, 1500, 2000 and 2500m. Regions with elevation anomalies larger than 200m are shaded, and with anomalies larger than 1000m are dark shaded.

Figure 3. LGM change in DJF air temperature ($^{\circ}\text{C}$) simulated by LMD4ter (top panel) and LMD5.3 (bottom panel). Isolines are represented for temperature anomalies of +2, 0, -5, -10, -20, -30, -40 $^{\circ}\text{C}$. Regions with temperature anomalies below 5 $^{\circ}\text{C}$ are shaded.

Figure 4. LMD5.3: Heat transfer coefficient between surface and atmosphere, over the continent, normalized by the neutral value, as a function of the Richardson number and for different values of z/z_0 . The horizontal solid line shows the non-dependency on the vertical stability of the transfer coefficients for LMD4ter.

Figure 5. Present-day DJF air temperatures (Celsius) from the climatology of *Legates and Willmott* [1990b] (top panel), and simulated by LMD4ter (middle panel) and LMD5.3 (bottom panel). Isolines are represented for each 5 $^{\circ}\text{C}$.

Figure 6. MH change in DJF air temperature ($^{\circ}\text{C}$) simulated by LMD4ter and LMD5.3. From top to bottom, LMD4ter mean change, LMD4ter selected years, LMD5.3 mean change and LMD5.3 selected years. See text for details. Isolines are represented for -10, -3, -2, -1, -0.2, +0.2, +1, +2, +3, +10 $^{\circ}\text{C}$. Regions with temperature anomalies above +0.2 $^{\circ}\text{C}$ are shaded.

Figure 7. Dry static energy meridional transport by the stationary eddies for present-day climate (top panel) and MH minus present-day change (bottom panel). Observations from *Keith* [1995], solid line; simulations by LMD4ter, dashed line; simulations by LMD5.3, dotted line. Error bars on the estimate of the mean computed from a 95%-confidence Student variable are also presented.

Figure 8. LMD4ter: projections ($^{\circ}\text{C}$) of the DJF temperatures over the continents (north of 30°N) for each year l of the control simulation, C_l , and of the MH simulation, H_l , to the basis formed by the mean of the control years (**C**) and of the MH years (**H**). S represents the mean of the “selected” MH years (H2, H3, H4, H, H9, H11, H13).

Figure 9. LMD5.3: projections ($^{\circ}\text{C}$) of the DJF temperatures over the continents (north of 30°N) for each year l of the control simulation, C_l , and of the MH simulation, H_l , to the basis formed by the mean of the control years (**C**) and of the MH years (**H**). S represents the mean of the “selected” MH years (H2, H3, H4, H6, H7, H8, H9, H12, H13, H15).

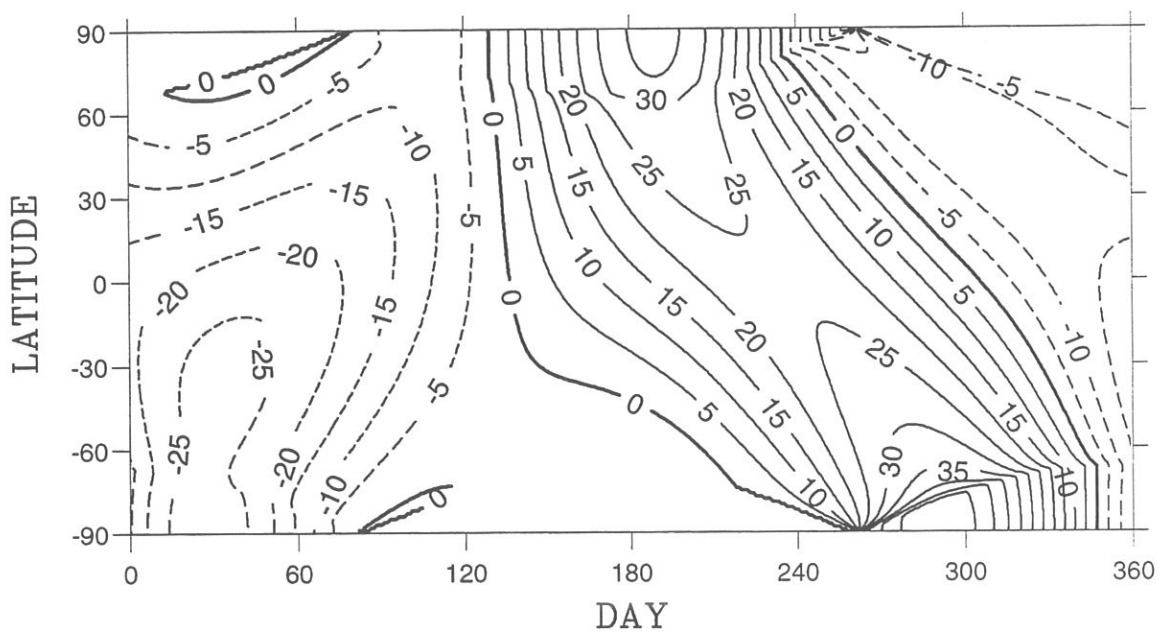
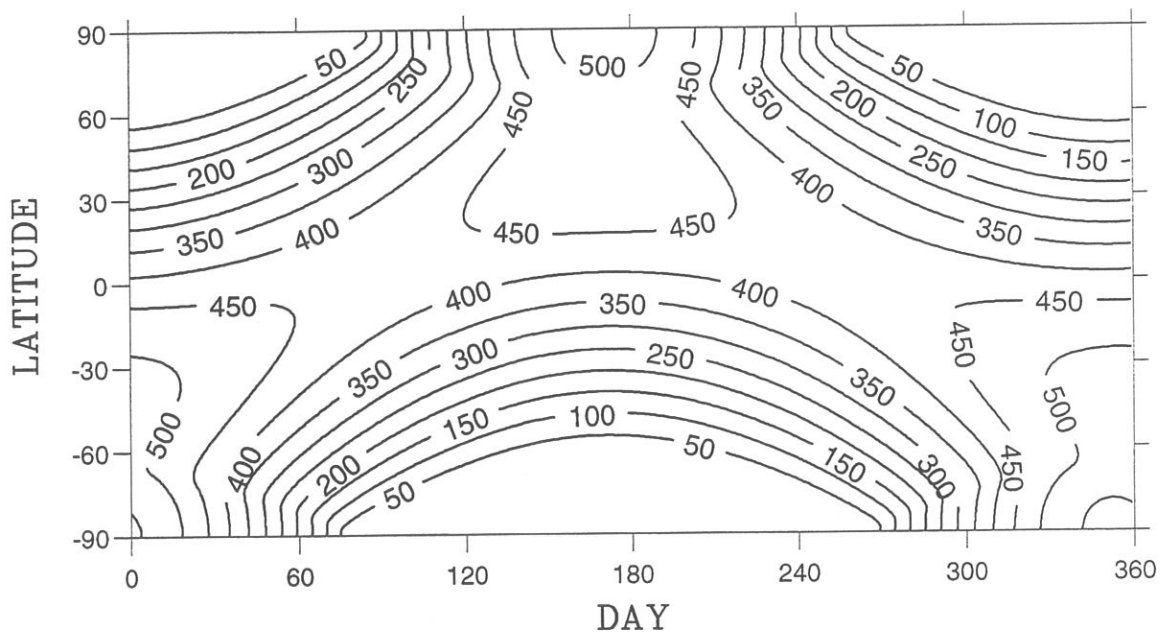


Figure 1:

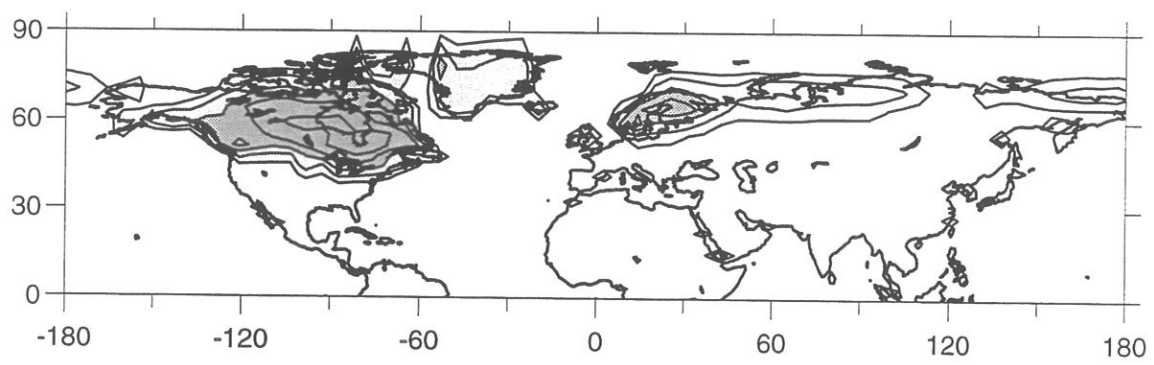
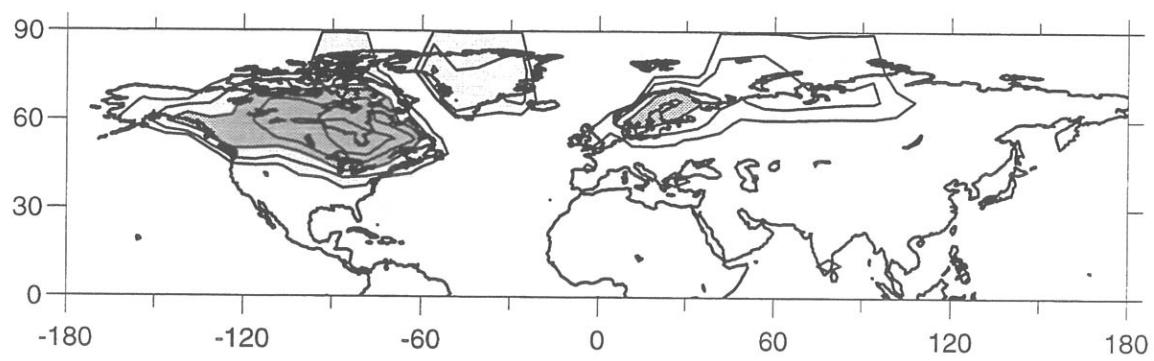


Figure 2:

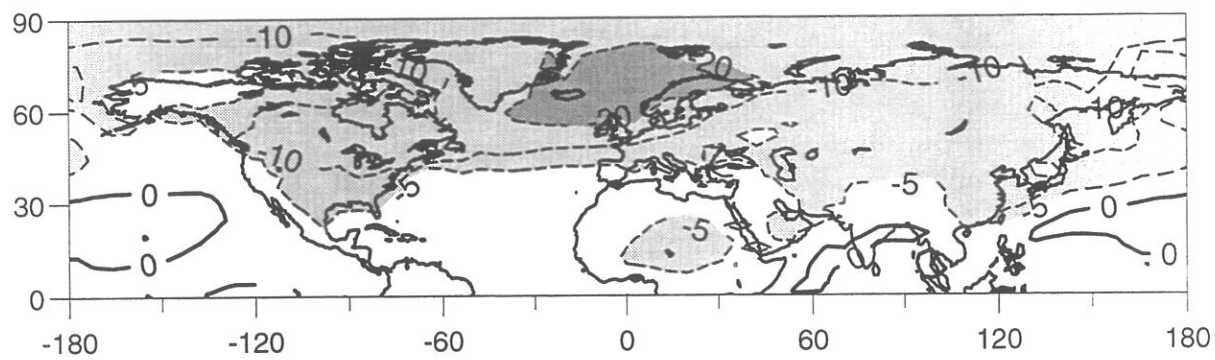
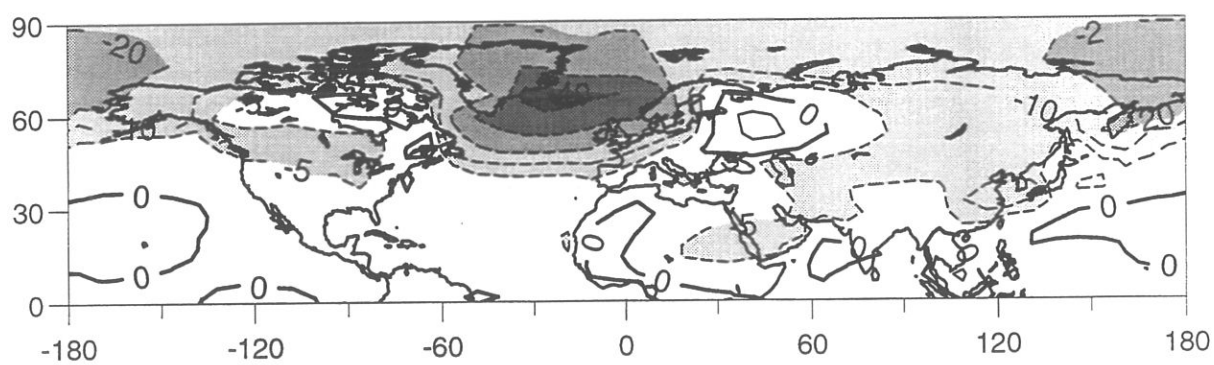
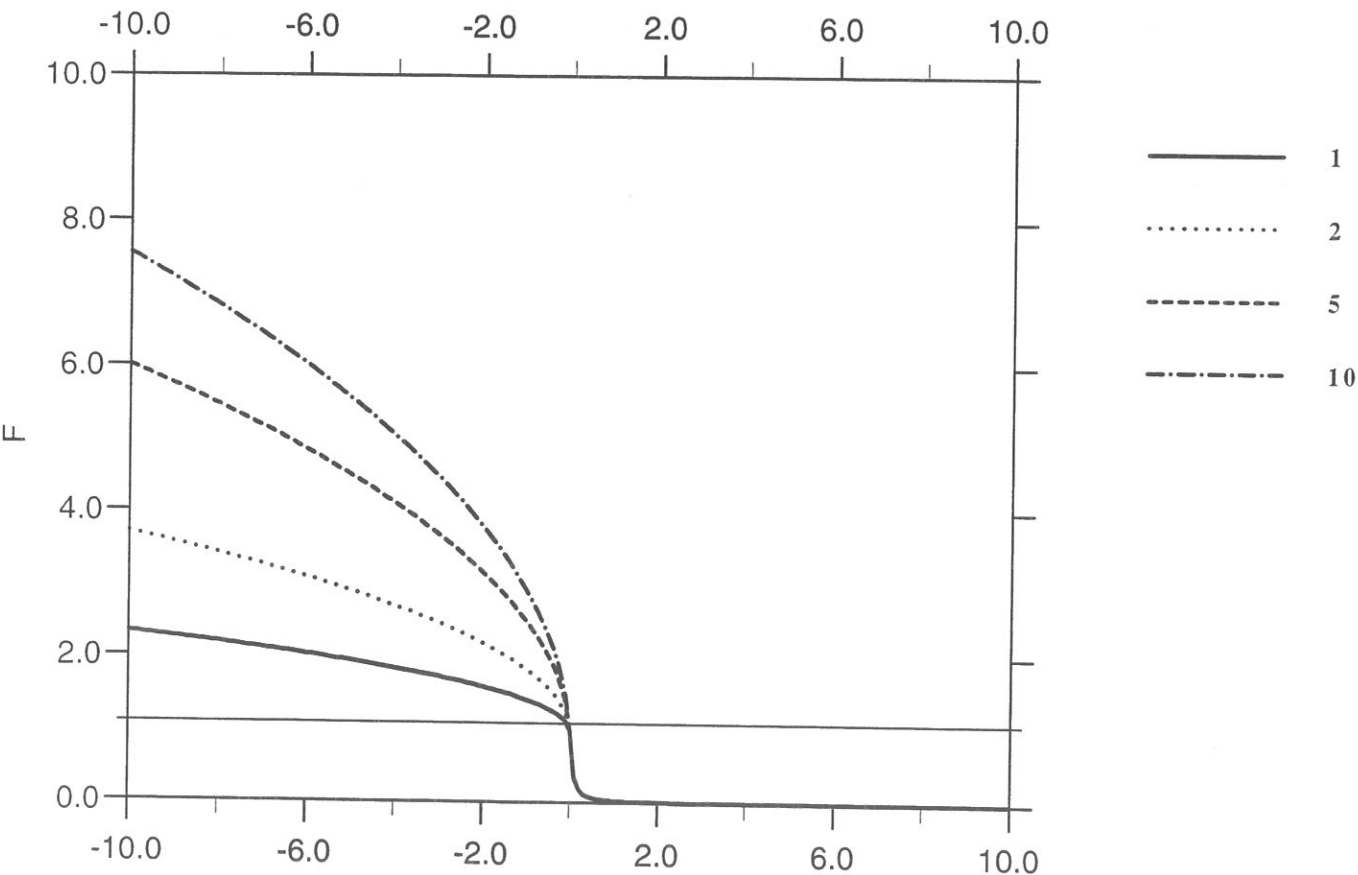


Figure 3:

Figure 4:



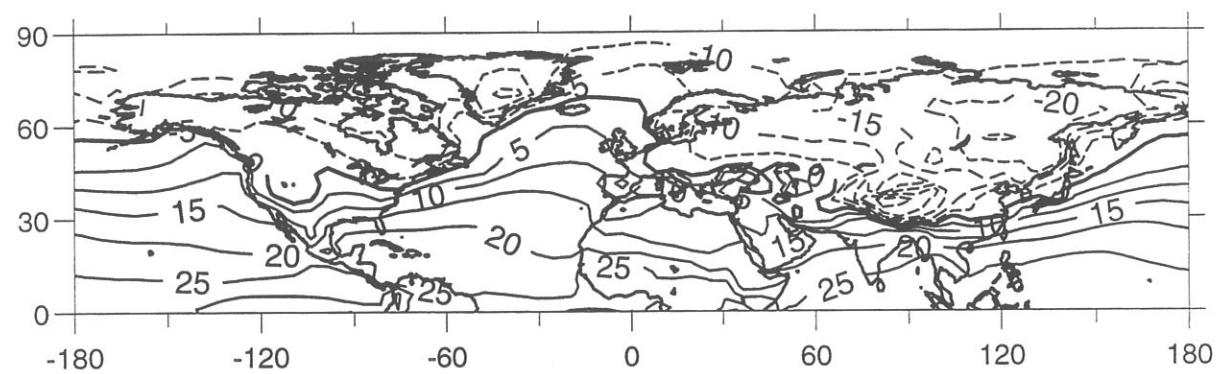
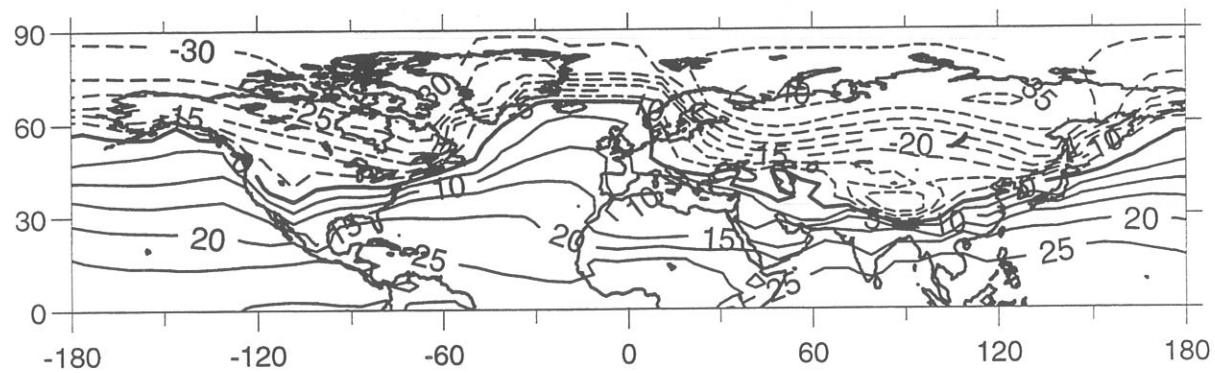
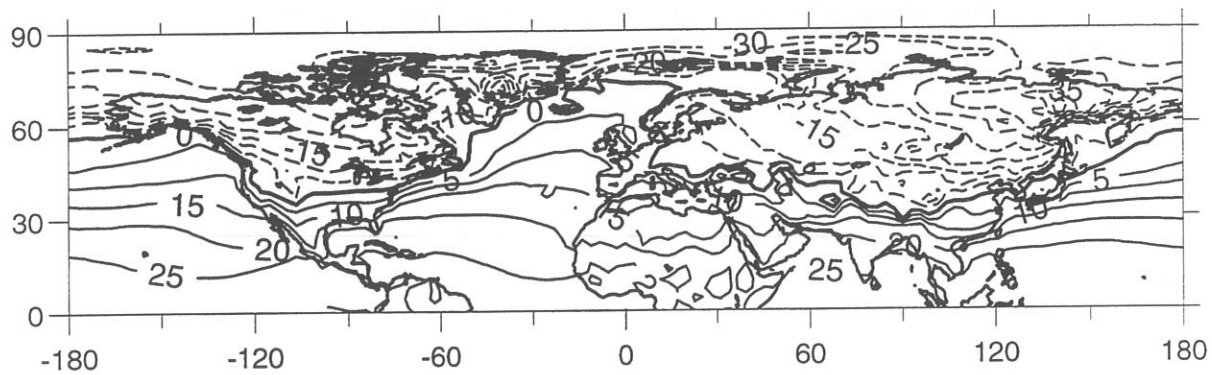


Figure 5:

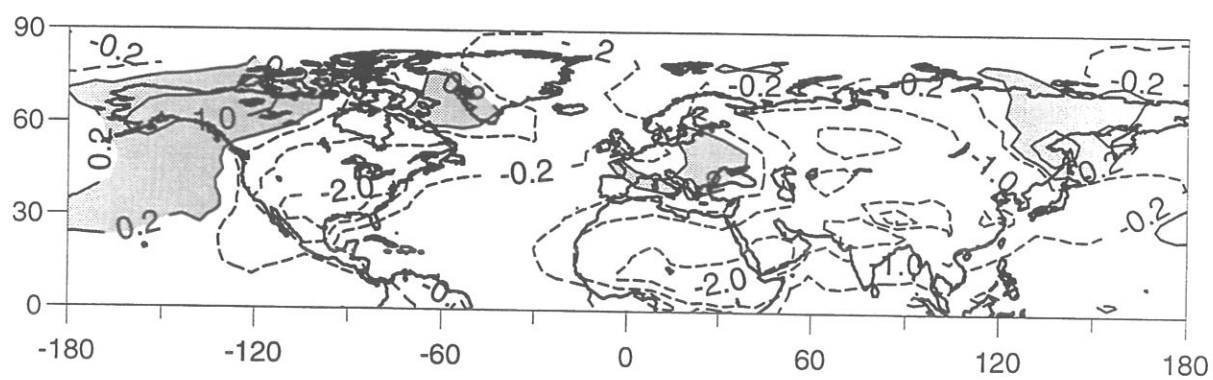
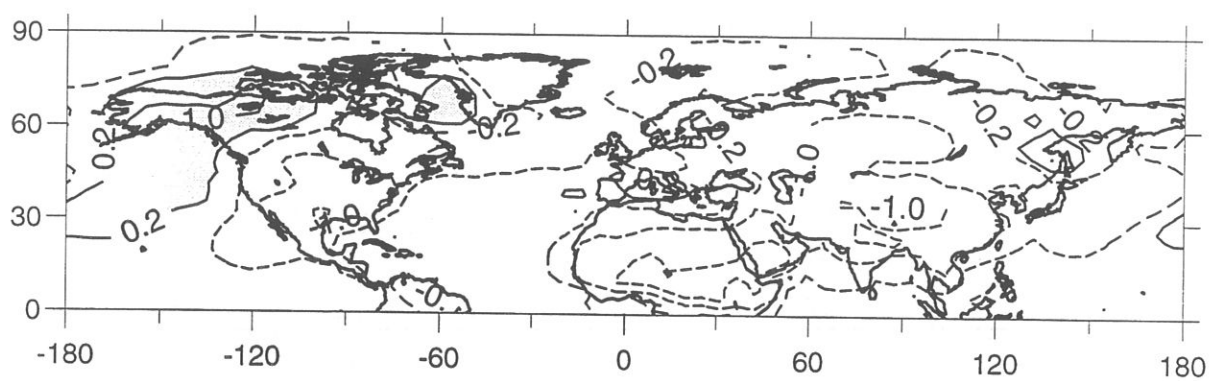
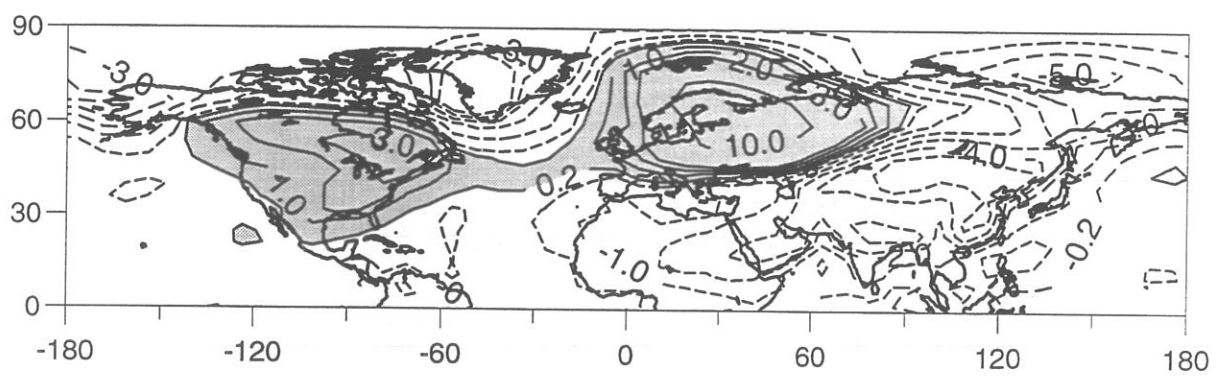
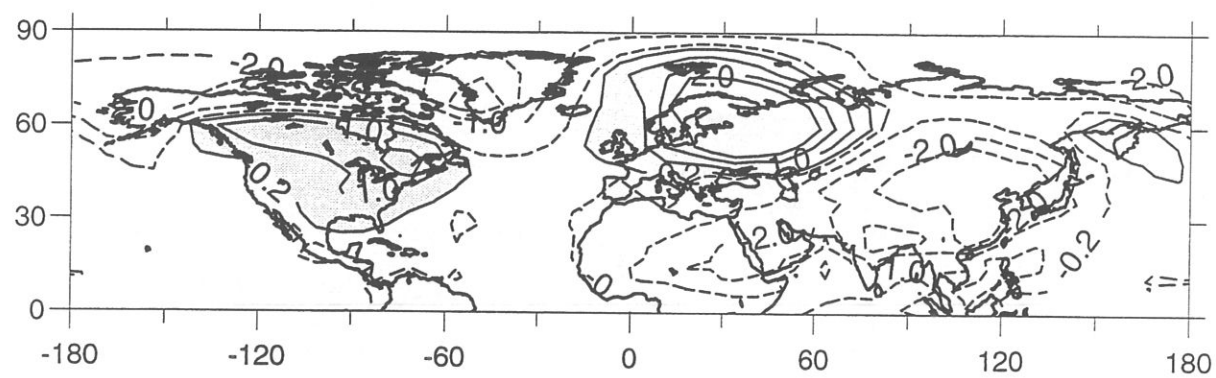


Figure 6:

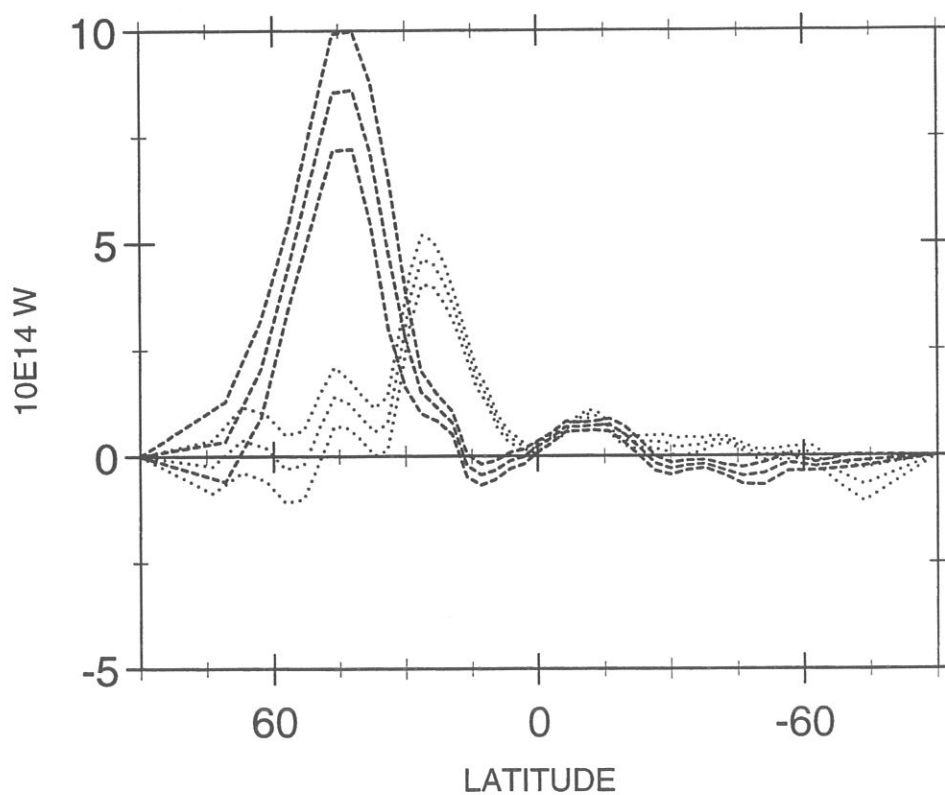
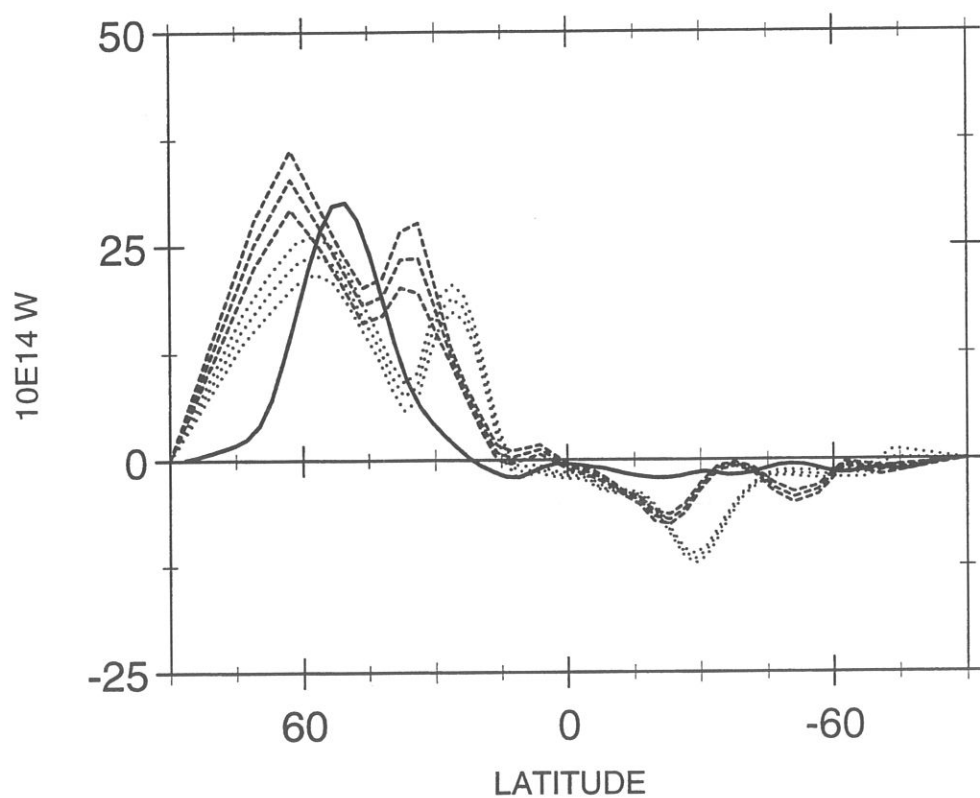


Figure 7:

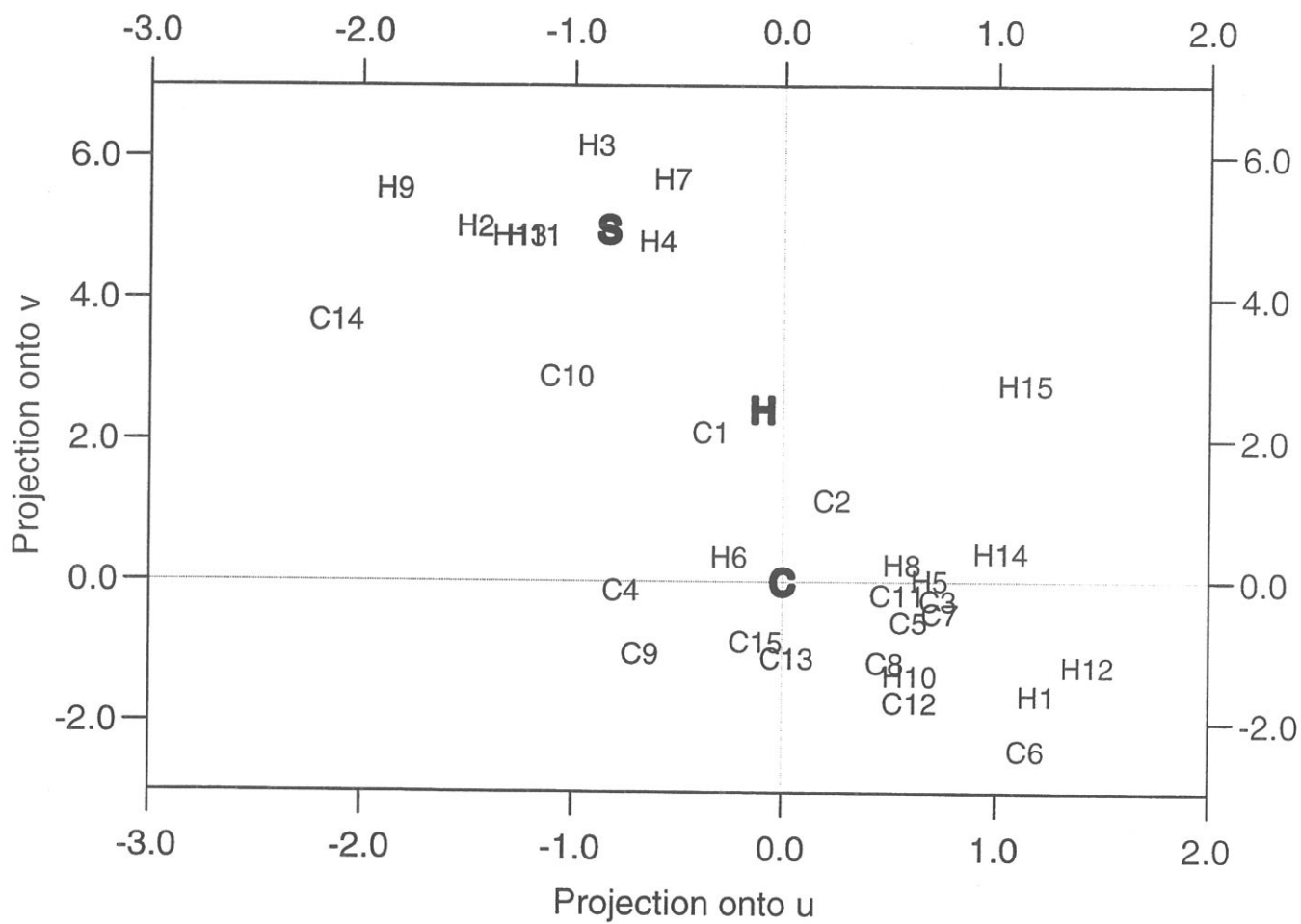


Figure 8:

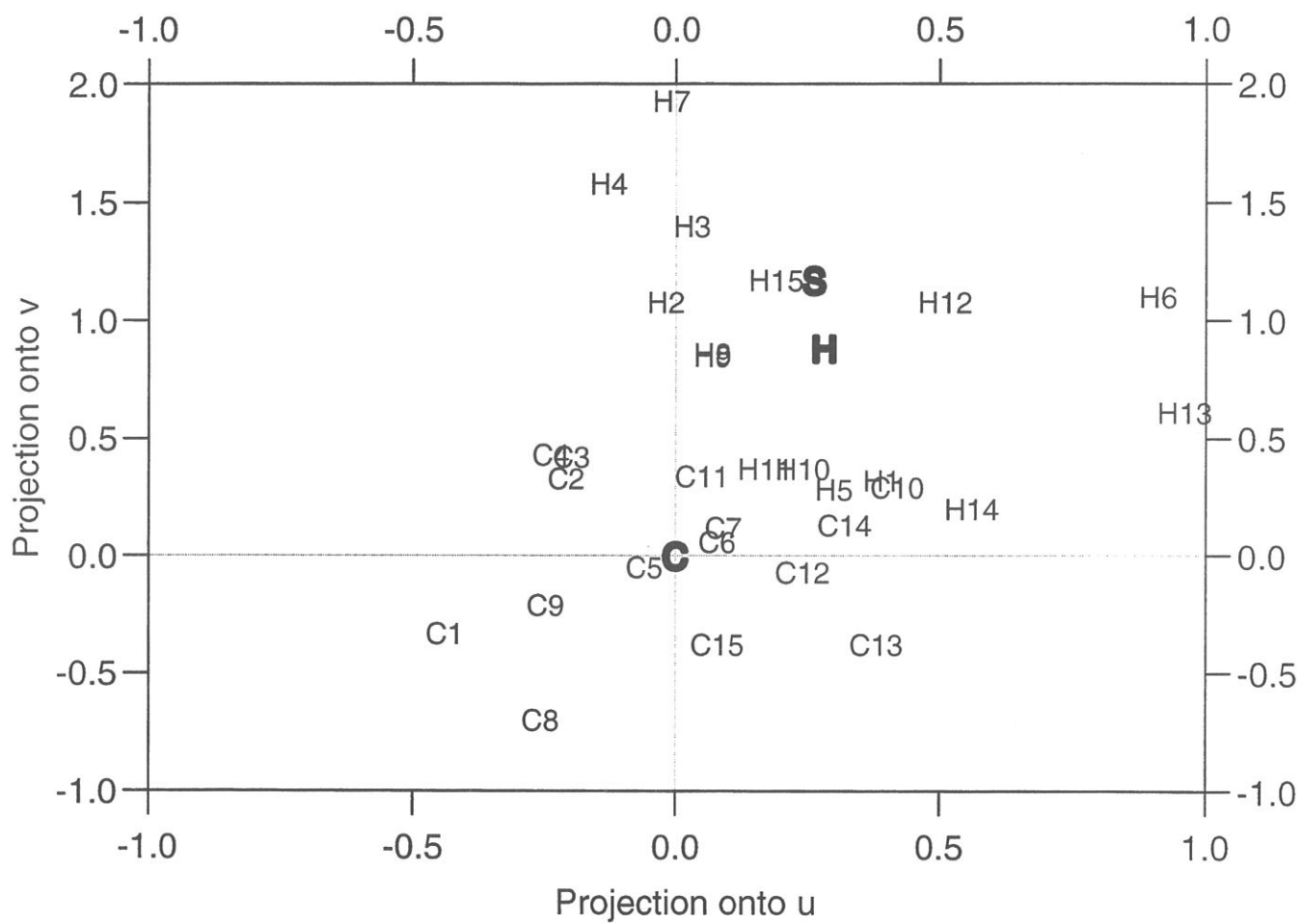


Figure 9:

	Present-day climate simulation		LGM climate simulation	
	LMD5.3	LMD4ter	LMD5.3	LMD4ter
Atmospheric energy budget (W/m^2)				
Net energy budget for the air column	+20.22	+67.50	-50.38*	-49.82*
Clear-sky radiative budget	-104.75*	-105.58*	-90.46	-84.07
Cloud radiative budget	-3.90	-14.33	-3.10	-6.17
Condensational heating (LP)	85.54	114.08	44.13	51.24
Sensible heat flux	43.33	73.33	-0.95*	-10.83
Surface energy budget (W/m^2)				
Surface net budget	-156.71	-198.80	-43.16	-18.48
Clear-sky surface radiative budget	-82.02	-73.68	-57.11	-45.44
Cloud surface radiative budget	+36.90	+45.02	+20.44*	+20.16*
Evaporation flux	-68.26	-96.81	-7.44	-4.03
Sensible heat flux	-43.33	-73.33	+0.95*	+10.83
Air stability				
Surface temperature ($^{\circ}\text{C}$)	5.83*	5.70*	-23.38	-28.20
Surface air temperature ($^{\circ}\text{C}$)	2.71*	2.84*	-16.32	-27.88
Richardson number	-1.06	-0.72	+9.20	+3.06
Surface transfer coefficients ($\times 10^3$)	0.24	1.40	0.12	1.40

Table 1:

Atmospheric energy (W/m^2)	Present-day climate simulation		Holocene minus present-day	
	LMD5.3	LMD4ter	LMD5.3	LMD4ter
Net budget for the air column	-95.73*	-95.50*	-1.83	-8.00
Clear-sky radiative budget	-103.86	-87.23	-0.35*	-4.93
Cloud radiative budget	-8.64	-10.59	-0.34	-1.07
Condensational heating (LP)	+39.77	+35.80	-0.86*	+0.55*
Sensible heat flux	-23.00	-33.48	-0.28	-2.55
Surface energy budget (W/m^2)				
Net budget for the surface	+0.56*	+0.29*	-0.15*	-0.03*
Clear-sky surface radiative budget	-40.84	-48.28	-1.11	-2.98
Cloud surface radiative budget	+22.28	+19.70	+0.11*	+1.15
Evaporation flux	-3.88	-4.61	+0.57	-0.75
Sensible heat flux	+23.00	+33.48	+0.28	+2.55
Atmospheric stability				
Surface temperature ($^{\circ}\text{C}$)	-19.80	-23.61	-0.67	+1.79
Surface air temperature ($^{\circ}\text{C}$)	-12.10	-22.90	-0.40	+1.82
Richardson number	+9.50	+4.65	+1.16	-0.15*
Surface transfer coefficients ($\times 10^3$)	0.61	7.00	-0.08	0.00

Table 2:

Déjà paru :

- 1 : **Janvier 1998** Agnès Ducharne, Katia Laval and Jan Polcher,
Sensitivity of the hydrological cycle to the parameterization of soil hydrology in a GCM
- 2 : **Janvier 1998** Marina Lévy, Laurent Mémerly and Jean-Michel André ,
Simulation of primary production and export fluxes in the Northwestern Mediterranean Sea